Passive vibration control of cylindrical offshore components using pipe-in-pipe (PIP) concept: An analytical study

Article *in* Ocean Engineering · September 2017

DOI: 10.1016/j.oceaneng.2017.06.063

CITATIONS
10

READS
552

3 authors, including:

Hamid Matin Nikoo
Atkins Global
12 PUBLICATIONS **88** CITATIONS
SEE PROFILE

Kaiming Bi
Curtin University
117 PUBLICATIONS **1,348** CITATIONS
SEE PROFILE

Ocean Engineering 142 (2017) 39–50

Contents lists available at ScienceDirect

Ocean Engineering

journal homepage: www.elsevier.com/locate/oceaneng

Passive vibration control of cylindrical offshore components using pipe-in-pipe (PIP) concept: An analytical study

Hamid Matin Nikoo, Kaiming Bi, Hong Hao*

Centre for Infrastructural Monitoring and Protection, School of Civil and Mechanical Engineering, Curtin University, Kent Street, Bentley, WA 6102, Australia

ARTICLE INFO

Keywords:
PIP system
Vortex-induced vibration control
Offshore cylindrical components
TMD
Optimal design

ABSTRACT

This paper aims to propose a design of using the revised PIP system to control vortex induced vibrations (VIV) of cylindrical structural components. Analytical studies are carried out to examine the effectiveness of the proposed method. To this end, the fluid-induced vibration of a single pipe is investigated and the equation of motion of the system is solved and validated by the experimental data. This single pipe system is then extended to the proposed PIP system and its dynamic behaviour under the excitation of vortex shedding is simplified as a Two-Degree-of-Freedom (2DoF) system. The optimal damping ratio and tuning frequency of the revised PIP system are obtained through a series of numerical searching technique and sensitivity analyses. Explicit formulae are also derived for practical ease of use. The governing equation of the system under VIV is solved in the time domain using the MATLAB/Simulink program. The responses of the single pipe system and the proposed PIP system due to vortex shedding are calculated and compared. Analytical results demonstrate that the proposed PIP system can significantly suppress the VIV of offshore cylindrical components. It could be then a cost-effective passive solution to suppress vibration of offshore cylindrical components.

1. Introduction

The exploration of energy resources has been moving into deep (above ~ 500 m) and ultra-deep (above ~ 1500 m) waters (Saint-Marcoux, 2014; Song et al., 2016). Various offshore structural components such as pipelines, risers and conductors are heavily used in the oil and gas industries to explore and transport these resources. During their service lives, these structures may be exposed to different vibration sources such as earthquake excitation and/or vortex shedding. Vortex induced vibration (VIV) is of special interests both in the industry and academic societies since many vortex shedding induced structural failures were repeatedly observed in offshores structures. Considerable research work has been conducted to attenuate such destructive vibrations (Choi et al., 2008; Raghavan et al., 2008; Rashidi et al., 2016; Williamson and Govardhan, 2004). These approaches can be generally divided into two broad categories: passive control and active control (Gad-el-Hak, 2000). Compared to the active control, passive control requires no external power to operate, it is, therefore, relatively less expensive and easier to install. Helical strakes and fairings have been most extensively used in engineering practices due to their effectiveness (Khorasanchi and Huang, 2014; Zeinoddini et al., 2015). For example, wind tunnel tests conducted by Zhou et al. (2011) showed that the intensity of vortices shed from the straked cylinder are weakened considerably and the vibration amplitude of the cylinder can be suppressed up to 98%. Experimental tests conducted by Gao et al. (2016) showed that fully-covered flexible risers with a helical strake can control the VIV in both uniform and linearly sheared currents up to 96% and 99%, respectively. However, the coverage of 75% and 50% yield the best comprehensive evaluation in uniform and linearly sheared currents. Allen (2003) experimentally investigated the performance characteristics of fairing for offshore risers. It was shown that fairings have much lower drag coefficient in comparison with helical strake and can significantly suppress the VIV. Besides helical strakes and fairings, many alternative methods have also been proposed by different researchers to effectively control VIV. Azmi et al. (2012) experimentally studied the effectiveness and mechanism of screen shroud to mitigate VIV amplitude and showed that this approach can suppress VIV by around 50%. The effect of porous media on the reduction of lift coefficient of cylinders undergoing VIV was numerically investigated by Zhao and Cheng (2010). Their results revealed that the reduction of lift coefficient depends on the thickness of the porous layer and Darcy number. Zhu and Yao (2015) carried out a series of numerical analyses to study the effectiveness of using control rods to suppress VIV and their results showed that using nine control

* Corresponding author.
E-mail address: hong.hao@curtin.edu.au (H. Hao).

http://dx.doi.org/10.1016/j.oceaneng.2017.06.063
Received 22 February 2017; Received in revised form 13 June 2017; Accepted 27 June 2017

rods can control VIV with a reasonable cost of inputs from an economic perspective. Kiu et al. (2011) studied the effect of surface roughness on the VIV response in a subcritical flow regime. Their results showed that by increasing the surface roughness, the maximum drag force, amplitude of response and width of lock-in region will decrease. Park et al. (2012) proposed a Passive Turbulence Control (PTC) device to control VIV, and their results indicated that the proposed system can suppress the maximum amplitude of VIV response up to 63%. Bernitsas and Raghavan (2014) patented a Surface Roughness Control (SRC) device to suppress VIV in high Reynold numbers regime; their experimental results showed that by attaching roughness strips, if distributed properly, noticeable reduction of VIV can be achieved. The effect of surface roughness on the VIV response of a flexible cylinder with large aspect ratio was experimentally studied by Gao et al. (2015). It was concluded that surface roughness has an important role in VIV response; a rough cylinder has a larger vortex shedding frequency with a narrower lock-in region and lower displacement response. A series of experimental tests conducted by Owen et al. (2001) showed that attaching hemi-spherical bumps (caps) with a constant longitudinal spacing and an angular separation of 45° can reduce drag force and VIV response up to 25%. They also reported a drag and VIV reduction for a wavy circular cylinder with a sinuous axis up to 47%. Assi et al. (2009) studied the effectiveness of a series of free to rotate splitter plates including single splitter plate, double splitters plates and parallel plates. The results showed that a maximum drag reduction of up to 38% can be achieved with parallel plates.

Although many afore-mentioned devices have been applied in engineering practices, certain drawbacks of these devices may considerably affect their performances especially when they are located in the deep and ultra-deep waters. For example, some devices (e.g. helical strake) usually impose an additional hydrodynamic drag force to the structure; some others (e.g. shrouds and axial slats (Kumar et al., 2008)) are expensive to manufacture, not easy to install, susceptible to marine growth and prone to storm damage, etc. It is, therefore, difficult to reach a reasonable balance between the efficiency, simplicity and cost. It is important to develop more efficient, cost effective and practical passive control devices to effectively control VIV.

A conventional PIP system comprises an internal insulated pipe (product pipe) which carries product flow and an outer pipe (sleeve pipe) which provides mechanical protection against the high external hydrostatic pressure and other mechanical damages (Bai and Bai, 2005). Thermal insulation layers are normally wrapped around the inner pipe to keep the temperature of the product. Centralizers which are used to centralize the inner pipe to prevent possible damage to the thermal insulation layer during installation, are normally installed along the pipe with an interval varying from 2 to 12 m (Bai and Bai, 2012). Extensive research works have been carried out on the conventional PIP system, and these works mainly focused on the structural instabilities such as the buckling of the system (e.g. Alrsai and Karampour (2016), Kyriakides (2002), Wang et al. (2015) and Zheng et al. (2014)). More recently, Bi and Hao (2016) slightly revised the conventional system and proposed a novel PIP system by replacing the hard centralizers with soft springs and dashpots. This revised PIP system was simplified as a structure-TMD system with the outer pipe acting as the main structure and the inner pipe performing as the TMD. This system was then proposed to mitigate seismic induced vibrations of subsea pipelines and numerical analyses were carried out to examine the effectiveness of the proposed method. Numerical results showed that this revised system can significantly suppress seismic induced vibrations of both the inner and outer pipes (Bi and Hao, 2016). This novel system takes advantage of the special structural layout of conventional PIP system. It does not vary too much from the traditional design, it is not much more expensive, and therefore is believed having great application potential.

This paper proposes a passive design based on revised Pipe-in-pipe (PIP) system to control the offshore cylindrical components under VIV. As will be demonstrated by the analytical results in the present study, this proposed system can significantly suppress VIV with slight revisions of the conventional PIP system. Analytical investigation is carried out to examine the effectiveness of the proposed method. Section 2 presents the mathematical model of a single cylinder under vortex shedding. The equation of motion of this single pipe system is solved and validated by the experimental data. This single pipe system is then extended to the modified PIP system in Section 3 where the equation of motion of the modified PIP system under VIV is derived. A MATLAB Simulink code is developed to solve the governing equation. To obtain the optimized connecting system, a series of sensitivity analysis is carried out to derive the explicit formulae for optimal spring stiffness and dashpot coefficients. The responses of the conventional and modified PIP systems subjected to vortex shedding are calculated in Section 4 and the effectiveness of the proposed design is discussed in that section.

2. Mathematical modelling of a single cylinder under VIV

Extensive efforts have been made to study the oscillating behaviour of circular cylinders under VIV. Comprehensive review of these methods can be found in Sarpkaya (2004) and Williamson and Govardhan (2008). There are mainly three approaches to investigate the VIV phenomena including numerical simulations, semi-empirical models and experimental tests. In the numerical simulations, the equation of fluid motion, known as the Navier-Stokes equation, is directly solved. This method is quite expensive in terms of computational cost and time consumption. Consequently, several alternative methods have been proposed to more efficiently solve this problem. For example, the phenomenological models or wake oscillator models, Single Degree of Freedom (SDOF) and force-decomposition models are widely used as the alternatives (Gabbai and Benaroya, 2005). The main difference between the alternative approaches and the direct numerical simulation is that the time-dependent behaviour of the fluid at the rear of the structure is modelled rather than being directly computed. For example, in the wake oscillator models, the displacement of the mounted body and wake oscillations are coupled through a pair of non-dimensional differential equations, i.e., the equation of the cylinder's motion and van der Pol oscillator (Facchinetti et al., 2004; Farshidianfar and Zanganeh, 2010). SDOF model, on the other hand, employs a single ordinary differential equation to describe the in-plane cross-flow oscillation of the body. In the force-decomposition models, the fluid force is split into an excitation and a reaction part that can define all the motion-dependent force components (Gabbai and Benaroya, 2005). The force-decomposition approach, which relies on experimental measurements of certain components of fluid forces, is in essence an SDOF method. This method can accurately describe and simulate experimental tests and thus is of great interest to study the nature of VIV, especially when strong computational and practical limitations arise respectively for numerical and experimental simulations. Moreover, it is believed that SDOF models are reasonably accurate for the purpose of evaluating the maximum VIV responses; therefore, they are sufficient for most wind and ocean engineering applications (Goswami et al., 1993). In this paper, the force-decomposition method is employed to study the cylindrical offshore structures under VIV.

2.1. Equation of motion

The equation of cross flow vibration (y) of an elastically-mounted rigid cylinder with diameter D under VIV oscillations can be written as (Gabbai and Benaroya, 2005):

$$m\ddot{y} + 2m\omega_n\zeta_s\dot{y} + m\omega_n^2 y = F_{fluid}(t) = F_L - F_R \quad (1)$$

where m is the mass of the oscillating system, ω_n is the natural

frequency of the structure and ζ_s is the structural damping ratio. The dot over the symbols denotes differentiation with respect to time. The time-dependent term $F_{fluid}(t)$ can be further divided into two components: the excitation or lift force (F_L) and the fluid reaction (F_R). The above equation can be re-written in a non-dimensional form as follows:

$$\ddot{y} + 2\omega_n\zeta_s\dot{y} + \omega_n^2 y = \beta\omega_s^2 C_{fluid}(t) \quad (2)$$

where $C_{fluid}(t)$ is the time-varying fluid coefficient on the oscillating structure defined by $C_{fluid}(t) = C_L - C_R$. Where, C_L and C_R are the vortex lift and reaction coefficients, respectively, ω_s is Strouhal frequency which is defined as below:

$$\omega_s = 2\pi f_s = 2\pi S_t U/D \quad (3)$$

where S_t is the Strouhal number and U is the free-stream velocity of the flow; β is a mass parameter or inverse Skop-Griffin parameter:

$$\beta = \rho D^2/8\pi^2 S_t^2 m \quad (4)$$

in which ρ is the fluid density. When the cylinder is vibrating within the lock-in region, in which the wake formation and fluctuating motion have a frequency near to the structural vibration frequency, the fluctuating transverse and total fluid force coefficient is nearly sinusoidal. So the total fluid coefficient can be expressed as:

$$C_{fluid}(t) = C_F \sin(\omega t + \varphi) \quad (5)$$

where φ is the phase difference between the fluid force and displacement of the cylinder. After substituting Eq. (5) into Eq. (2), the equation of cylinder motion becomes:

$$\ddot{y} + 2\omega_n\zeta_s\dot{y} + \omega_n^2 y = \beta\omega_s^2 C_F \sin(\omega t + \varphi) \quad (6)$$

Eq. (6) can accurately simulate a cylinder under VIV when the empirical values C_F are obtained from the experimental results.

2.2. Vibration simulation of a single cylinder under VIV

In this section, the SDOF model is used to simulate an available experimental test carried out by Rahman (2015) aiming at developing a validated analytical model for further analysis (the analysis of the proposed PIP system). Fig. 1 shows the schematic view of the experiments.

A towing tank with the length, width and depth of 50 m, 1.25 m and 1.10 m, respectively was used in the tests. The testing cylinder was towed by the towing cable in the still water. The cylinder was mounted to a four-armed pendulum system, and two linear springs were used to restrain the cylinder in the transverse direction. A set of tension load cells were used to measure the hydrodynamic forces acting on the rig. It should be noted that the experiment focused on the cross-flow vibration of the cylinder and the motion in the in-line direction was ignored. Moreover, the experiment was conducted in the subcritical flow region with Reynolds numbers ranging from 7.4×10^3 to 2×10^5, corresponding to the range of reduced velocity $U_r (U_r = U/f_n D; \omega_n = 2\pi f_n)$ from 2 to 14 (Rahman, 2015; Rahman and Thiagarajan, 2013). Detailed information regarding the experimental setup can be found in Rahman (2015). To consider the effect of aspect ratio (the proportion of cylinder length to the diameter), four cases (with L/D = 13, 10, 7.5 and 5) are examined in the present study using the parameters listed in Table 1 and Table 2, and the fluid coefficients C_F obtained from the tests as shown in Fig. 2.

As can be seen from Table 1, the Strouhal numbers obtained in the tests are between 0.098 and 0.146 and they depend on the aspect ratio. On the other hand, it is widely known that a Strouhal number for a circular cylinder is around 0.2. Two reasons result in the different and relatively small Strouhal numbers in the tests: (i) when the aspect ratio is small, the three-dimensional (3D) wake effect can trigger the wake turbulent region around the cylinder (Rahman et al., 2016) and (ii) different aspect ratios can cause changes to the correlation length of vortex shedding (Norberg, 1994). The obtained results are consistent with the work done by Gouda (1975), in which it was indicated that a steady value of Strouhal number of 0.2 can be governed when the cylinder aspect ratio is larger than nearly 50. Moreover, using end plate can also cause a significant influence on the Strouhal frequency as extensively discussed by Szepessy and Bearman (1992).

Fig. 4 compares the normalized amplitudes of the cylinder oscillations (A_y/D) obtained from the experiments and the analytical results over a range of reduced velocities. It can be seen that there is a good agreement between the experimental and semi-empirical results, which demonstrate the accuracy of the dynamic Simulink model as shown in Fig. 3. The comparisons also indicate that the accuracy of the SDOF model is slightly decreased for lower aspect ratios (especially in

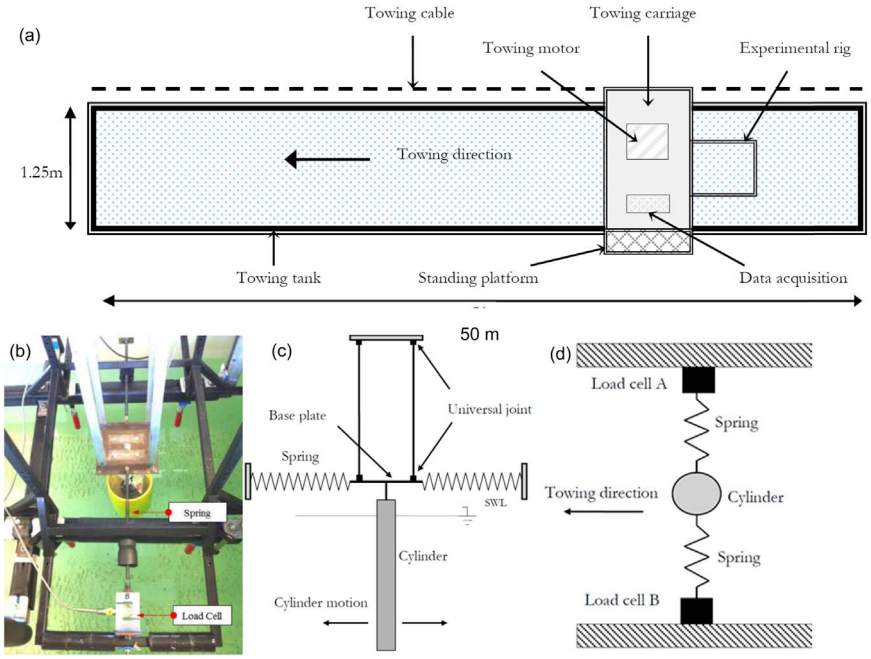

Fig. 1. Experimental setup of a single cylinder under VIV: (a) Hydraulic towing tank; (b) Force measurement device; (c) and (d) Schematic diagrams of the pendulum rig (Rahman, 2015).

Table 1
Experimental matrix performed in (Rahman, 2015).

	$L(m)$	$D(m)$	L/D	$k(N/m)$	$m(kg)$	$m_{osc,in\ water}(kg)$	$f_n(Hz)$	ζ	S_t
Exp. 1	0.78	0.06	13	245	5.73	3.53	0.99	0.031	0.146
Exp. 2	0.60	0.06	10	245	4.41	2.71	1.12	0.031	0.130
Exp. 3	0.60	0.08	7.5	245	7.84	4.82	0.865	0.036	0.111
Exp. 4	0.40	0.08	5	245	5.22	3.21	1.035	0.032	0.098

Table 2
The range of examined current velocity and corresponding vortex shedding frequency (Rahman, 2015).

	L/D	$U(m/s)$	$f_s(Hz) = S_t U/D$	f_s/f_n
Exp. 1	13	[0.12 0.98]	[0.29 2.38]	[0.29 2.41]
Exp. 2	10	[0.14 1.10]	[0.30 2.38]	[0.27 2.13]
Exp. 3	7.5	[0.14 1.10]	[0.19 1.51]	[0.22 1.75]
Exp. 4	5	[0.17 1.37]	[0.21 1.68]	[0.20 1.62]

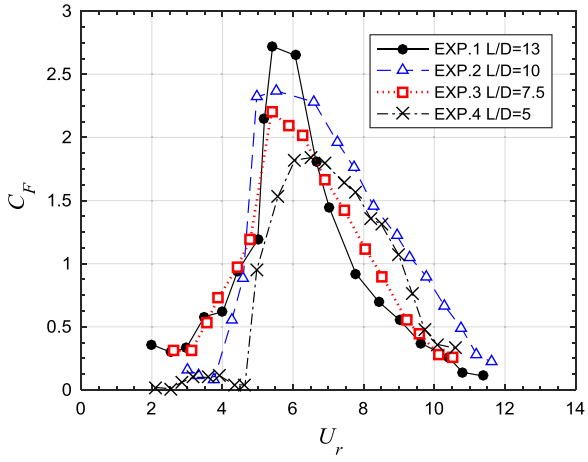

Fig. 2. Root Mean Square of the observed fluid coefficient C_F from the experimental tests (Rahman, 2015).

Fig. 4(d)). This is because when the aspect ratio is small, the vortex formation frequency and the corresponding lift force change, which lead to the instability of the wake structure and further arise the 3D effects (Rahman et al., 2016). The SDOF model, which in essence a simplified single ordinary differential equation to describe the cross-flow VIV response, then will be difficult to accurately capture all the features of fluid behaviour. It is also worth mentioning that nonlinear effects associated with VIV phenomena and added mass variation in the lock-in region (Gabbai and Benaroya, 2005) are considered by using the varying fluid coefficient (C_F) obtained from experimental test (Rahman, 2015; Rahman and Thiagarajan, 2013) (see Fig. 2).

A time-domain Simulink model (Fig. 3) is developed in MATLAB to solve Eq. (6). On the left side of the Simulink model, the external fluid force including two feedback loops is entered to the system. The first one refers to the cylinder velocity and it is multiplied by the damping, and the second loop stands for the cylinder displacement, which is multiplied by the stiffness of the spring. The symbol $\frac{1}{s}$ is an integrator block, which outputs the value of the integral of its input signal with respect to time. All the parameters including the mass, damping and stiffness coefficients are the same as those in the experimental test (Rahman, 2015).

Fig. 4 also shows that within a certain reduced velocity range (normally known as the lock-in or synchronization region), the oscillating amplitudes of the cylinder are significant, which means there is a broad range, but not just one particular frequency, that can cause significant vibrations to the cylinder. The suppression of VIV is therefore important for the cylindrical offshore structures. The lock-in regions are different for different aspect ratios, but generally speaking for the investigated aspect ratios, lock-in phenomena take place when the reduced velocity is between 5 and 9.

It should be noted that some assumptions are made in the derivation of Eq. (6) (Gabbai and Benaroya, 2005). They are: 1) the cylinder is rigid and the flow around the body is fully correlated and two-dimensional; and 2) the dynamic behaviour of the flow field around the oscillating body and the effect of geometry are not considered. This model, therefore, might not be a comprehensive model. However, it is fairly accurate for the preliminary study to examine the effectiveness of the proposed system especially considering the good matches between the analytical and experimental results as shown in Fig. 4. This semi-empirical model will be extended to study the behaviour of modified PIP system under VIV in the following sections.

3. Optimized PIP to control vibration of cylindrical structures caused by VIV

In this section, the simplified governing equation of the modified PIP system subjected to VIV is firstly presented and then the optimal values of the spring stiffness and damping coefficient are investigated.

3.1. Basic governing equations of PIP system and method of solution

Fig. 5 shows the structural and simplified analytical models of the modified PIP system. As shown in Fig. 5(a), the coaxial inner and outer

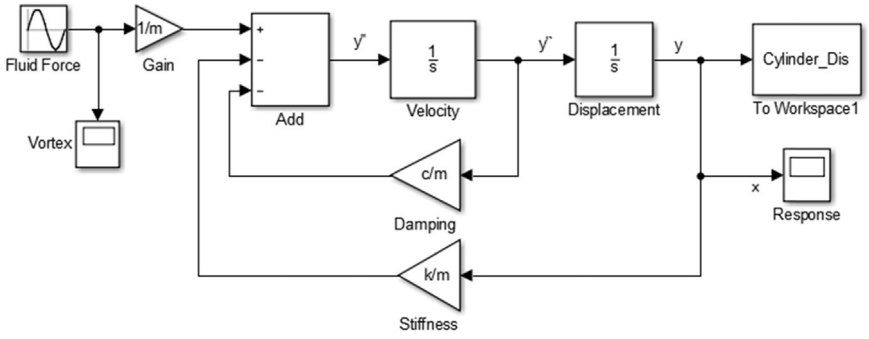

Fig. 3. Schematic of the dynamic Simulink model for a single cylindrical structure under VIV.

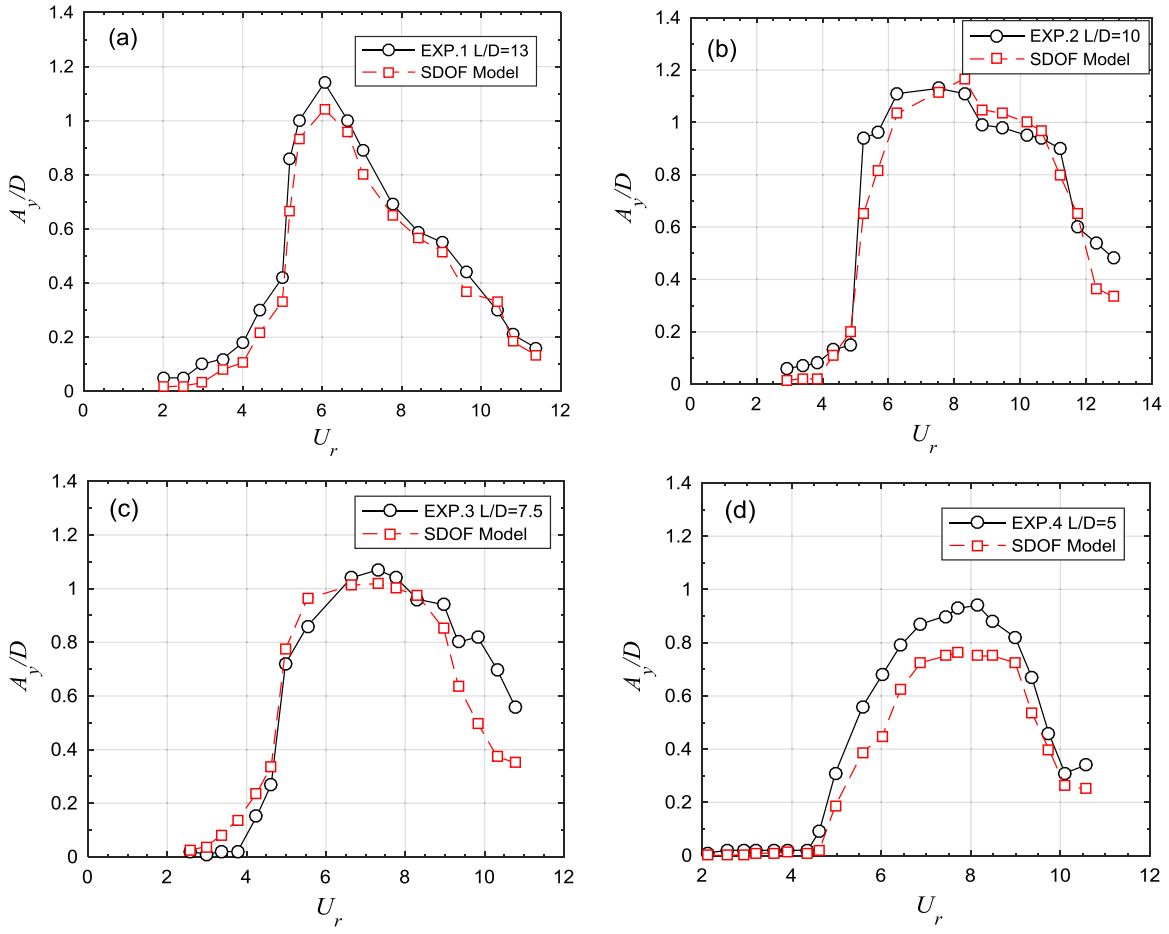

Fig. 4. Comparisons of the normalized amplitudes obtained from the experimental data and the analytical solutions for different aspect ratios (a) $L/D = 13$ (b) $L/D = 10$ (c) $L/D = 7.5$ and (d) $L/D = 5$. (For interpretation of the references to color in this figure, the reader is referred to the web version of this article)

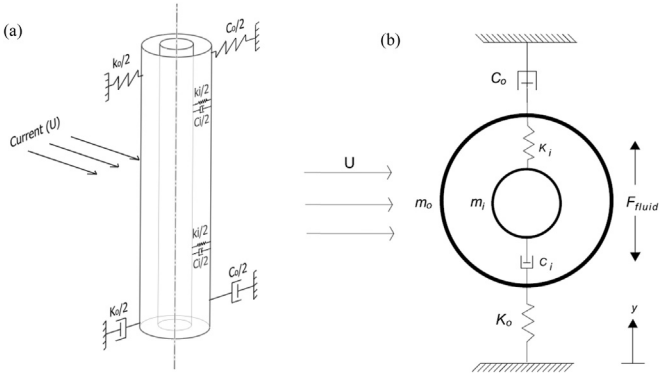

Fig. 5. Structural and analytical models of the modified PIP system (a) structural model and (b) analytical model.

pipes are connected by the springs and dashpots. This system can be simplified as a two-degree-of-freedom (Two-DOF) system consisting of a primary oscillator (the outer pipe) and an auxiliary TMD (the inner pipe) as shown in Fig. 5(b). It should be noted that for a conventional structure-TMD system, the mass ratio between the TMD and the main structure is normally in an order of 1–5% percent. For this modified PIP system, the mass ratio, however, can be much larger and in certain cases the mass of the inner pipe can be almost the same as the outer pipe. This system is normally regarded as a non-conventional TMD system (Bi and Hao, 2016).

As shown in Fig. 5(b), the primary oscillator is characterized by a mass m_o, a linear stiffness k_o and a constant viscous damping coefficient c_o. The natural frequency and viscous damping ratio of the primary structure are therefore $\omega_o = \sqrt{k_o/m_o}$ and $\zeta_o = c_o/2\sqrt{k_o m_o}$. Similar to the main system, the corresponding parameters for the TMD system are m_i, k_i, c_i, with $\omega_i = \sqrt{k_i/m_i}$ and $\zeta_i = c_i/2\sqrt{k_i m_i}$.

When this system is subjected to the vortex shedding excited cross-flow vibration, the equation of motion can be expressed as:

$$\begin{bmatrix} m_o & 0 \\ 0 & m_i \end{bmatrix}\begin{Bmatrix} \ddot{y}_o \\ \ddot{y}_i \end{Bmatrix} + \begin{bmatrix} c_o + c_i & -c_i \\ -c_i & c_i \end{bmatrix}\begin{Bmatrix} \dot{y}_o \\ \dot{y}_i \end{Bmatrix} + \begin{bmatrix} k_o + k_i & -k_i \\ -k_i & k_i \end{bmatrix}\begin{Bmatrix} y_o \\ y_i \end{Bmatrix} = \begin{Bmatrix} F_{fluid}(t) \\ 0 \end{Bmatrix} \tag{7}$$

where y_o and y_i are the in-plane transverse displacements of the outer and inner pipes, respectively.

To facilitate the optimization of the spring stiffness and damping coefficient, it is convenient to define the mass ratio μ and tunning frequency ratio f as follows:

$$\mu = m_i/m_o \tag{8}$$

$$f = \omega_i/\omega_o = \sqrt{\frac{1}{\mu}\left(\frac{k_i}{k_o}\right)} \tag{9}$$

3.2. Optimum design of non-conventional tuned mass damper (TMD)

TMD systems have been widely used to attenuate the undesirable vibrations of engineering structures due to their simplicity (Dinh and Basu, 2015; Gutierrez Soto and Adeli, 2013). To make the system effective, the key factor is to obtain the optimal values of the spring stiffness and damping coefficient. Various methods have been proposed to estimate the optimal TMD parameters (e.g. harmony search (Bekdaş and Nigdeli, 2011) and equivalent linearization (Anh and Nguyen,

Table 3
Obtained optimal parameters for a TMD system with different mass ratios based on the numerical searching technique.

	$\zeta_o = 0.02$			$\zeta_o = 0.04$			$\zeta_o = 0.06$			$\zeta_o = 0.08$			$\zeta_o = 0.1$		
μ	ζ_i^{opt}	f^{opt}	N^{opt}	ζ_i^{opt}	f^{opt}	N^{opt}	ζ_i^{opt}	f^{opt}	N^{opt}	ζ_i^{opt}	f^{opt}	N^{opt}	ζ_i^{opt}	f^{opt}	N^{opt}
0.10	0.153	0.929	2.6243	0.153	0.926	2.2507	0.153	0.924	1.9634	0.153	0.921	1.7366	0.152	0.919	1.5536
0.15	0.184	0.899	2.1992	0.184	0.896	1.9327	0.184	0.893	1.7193	0.184	0.890	1.5451	0.184	0.887	1.4007
0.20	0.209	0.871	1.9319	0.209	0.868	1.7242	0.209	0.865	1.5536	0.209	0.862	1.4112	0.209	0.859	1.2910
0.25	0.230	0.845	1.7431	0.230	0.842	1.5729	0.230	0.839	1.4304	0.230	0.836	1.3096	0.230	0.833	1.2062
0.30	0.248	0.822	1.6004	0.248	0.818	1.4562	0.248	0.815	1.3337	0.248	0.812	1.2287	0.248	0.809	1.1377
0.35	0.264	0.800	1.4874	0.264	0.796	1.3623	0.264	0.793	1.2550	0.264	0.790	1.1619	0.264	0.787	1.0807
0.40	0.278	0.779	1.3951	0.278	0.776	1.2847	0.278	0.773	1.1890	0.278	0.769	1.1055	0.278	0.766	1.0320
0.45	0.291	0.760	1.3177	0.291	0.757	1.2190	0.291	0.754	1.1328	0.291	0.750	1.0569	0.291	0.747	0.9898
0.50	0.303	0.742	1.2517	0.303	0.739	1.1624	0.303	0.736	1.0839	0.303	0.732	1.0145	0.303	0.729	0.9527
0.55	0.314	0.725	1.1945	0.313	0.722	1.1130	0.313	0.719	1.0410	0.313	0.716	0.9769	0.313	0.713	0.9196
0.60	0.324	0.709	1.1442	0.323	0.706	1.0694	0.323	0.703	1.0028	0.323	0.700	0.9434	0.323	0.697	0.8900
0.65	0.332	0.695	1.0997	0.333	0.691	1.0305	0.333	0.688	0.9686	0.333	0.685	0.9132	0.332	0.683	0.8632
0.70	0.341	0.680	1.0598	0.341	0.677	0.9954	0.341	0.674	0.9377	0.341	0.671	0.8858	0.341	0.669	0.8387
0.72	0.344	0.675	1.0450	0.344	0.672	0.9824	0.344	0.669	0.9262	0.344	0.666	0.8755	0.344	0.663	0.8296
0.74	0.347	0.67	1.0308	0.347	0.667	0.9698	0.347	0.664	0.9150	0.347	0.661	0.8656	0.347	0.658	0.8207
0.76	0.351	0.664	1.0171	0.35	0.662	0.9578	0.35	0.659	0.9043	0.35	0.656	0.8560	0.35	0.653	0.8121
0.78	0.354	0.659	1.0040	0.354	0.656	0.9461	0.353	0.654	0.8939	0.353	0.651	0.8467	0.353	0.648	0.8038
0.80	0.357	0.654	0.9913	0.356	0.652	0.9349	0.356	0.649	0.8839	0.356	0.646	0.8377	0.356	0.643	0.7957
0.82	0.359	0.65	0.9791	0.359	0.647	0.9240	0.359	0.644	0.8742	0.359	0.641	0.8291	0.359	0.638	0.7879
0.84	0.362	0.645	0.9673	0.362	0.642	0.9135	0.362	0.639	0.8648	0.362	0.636	0.8206	0.362	0.634	0.7803
0.86	0.365	0.64	0.9559	0.365	0.637	0.9034	0.365	0.634	0.8558	0.364	0.632	0.8125	0.364	0.629	0.7730
0.88	0.367	0.636	0.9449	0.367	0.633	0.8935	0.367	0.63	0.8470	0.367	0.627	0.8046	0.367	0.625	0.7659
0.90	0.37	0.631	0.9342	0.37	0.628	0.8840	0.37	0.625	0.8384	0.37	0.623	0.7969	0.37	0.620	0.7589

2013)). It should be noted that most of these methods consider the conventional TMD system, i.e. the system with small mass ratio. Very limited studies reported the optimization of TMD system with large mass ratio. For example, Hoang et al. (2008) presented explicit formulas to optimize the TMD parameters with large mass ratio when the main system is subjected to earthquake loading, i.e. base excitation. For the modified PIP system, vortex shedding induced force is applied on the external pipe, i.e. on the main structural mass. The optimization formulas for this case are different from those presented in Hoang et al. (2008). To the best knowledge of the authors, no open literature presents straightforward explicit formulas for tuning parameters of the non-conventional TMD system (with high mass ratio) when the external force is applied on the main structure. The optimization of the modified PIP system is introduced in this section.

It is well known that the vibrations of cylindrical offshore components induced by vortex shedding include characteristics as follows. The current flow and vortex shedding frequency vary in space and time (ISO, 2015; Veritas, 2000). The vibration of cylindrical structures in steady current can be divided into different categories: (i) the forced vibration by Karman vortex shedding, which excites the structure at a dominant frequency; (ii) the vibration in the synchronization or lock-in region, which occurs not only near a dominant frequency but also over a broad range of input frequencies (current velocities); (iii) turbulence-induced vibration in which the structures are excited by a broad-band frequency out of the lock-in region and (iv) excitation induced by tip-vortices in the high flow velocity regime (Nakamura et al., 2013). Due to these reasons, there is a wide range of current velocities/vortex shedding frequencies, within which the oscillations should be suppressed as discussed in Section 2. The external force applied to the main system can be assumed as a stationary Gaussian random process with a constant power spectral density (PSD).

In the present study, the vibration amplitude of the external pipe is taken as the parameter to be suppressed (actually as demonstrated in Bi and Hao, 2016, the vibration of the inner pipe can be mitigated as well due to the large mass ratio of the system). For a TMD system subjected to a excitation with a constant PSD S_0, the mean square displacement of the external pipe (the objective function) can be expressed by Bakre and Jangid (2007):

$$\sigma_{y_o}^2 = \int_{-\infty}^{\infty} S_0 |H_{y_o}(\omega)|^2 d\omega \tag{10}$$

in which $H_{y_o}(\omega)$ is the frequency response function, and it has the following form:

$$H_{y_o}(\omega) = 1/\Delta m_o(-\omega^2 + 2i\zeta_i\omega_i\omega + \omega_i^2) \tag{11}$$

where

$$\Delta = \omega^4 - 2i[\omega_o\zeta_o + (1+\mu)\zeta_i\omega_i]\omega^3 - [\omega_o^2 + (1+\mu)\omega_i^2 + 4\omega_i\omega_o\zeta_i\zeta_o]\omega^2 + 2i\omega_i\omega_o[\omega_i\zeta_o + \omega_o\zeta_i]\omega + \omega_o^2\omega_i^2 \tag{12}$$

Substituting Eq. (11) into Eq. (10), the objective function ($\sigma_{y_o}^2$ or N) becomes (Bakre and Jangid, 2007):

$$N = \frac{1}{4}(I/L) \tag{13}$$

where

$$I = \zeta_i[1 - f^2(2+\mu) + f^4(1+\mu)^2] + \mu f^3\zeta_o + 4f^2\zeta_i^3(1+\mu) + 4f\zeta_i^2\zeta_o[1 + f^2(1+\mu)] + 4f^2\zeta_i\zeta_o^2 \tag{14}$$

$$L = [\mu f\zeta_i^2 + \zeta_i\zeta_o\{1 - 2f^2 + f^4(1+\mu)^2 + 4f^2\zeta_i^2(1+\mu) + 4f\zeta_i\zeta_o[1 + f^2(1+\mu)] + 4f^2\zeta_o^2\} + \mu f^3\zeta_o^2] \tag{15}$$

For an undamped primary structure, it is possible to obtain closed-form expressions for the optimum TMD parameters by solving the optimization condition equations:

$$\partial N/\partial f = 0, \partial N/\partial\zeta_i = 0 \tag{16}$$

However, for a damped primary system, Eq. (16) cannot be solved for the closed-form expressions and normally a numerical searching technique is adopted to obtain the optimal parameters (Bakre and Jangid, 2007; Salvi and Rizzi, 2015). For a given mass ratio (μ) and damping ratio of the main system (ζ_o), the numerical searching algorithm seeks the optimal frequency ratio (f^{opt}) and damping ratio of the TMD system (ζ_i^{opt}) in such a way that the objective function N, attains a minimum value.

Table 3 tabulates the obtained optimal parameters for the TMD

system and the corresponding response quantities for five different main system damping ratios (ζ_o = 0.02, 0.04, 0.06, 0.08, 0.1). The superscript *opt* indicates the optimal TMD tuning parameters.

It should be noted that the numerical searching technique itself is not new and many researchers have adopted this method to obtain the optimal TMD parameters. However, most of previous studies emphasized mainly on the small mass ratio as mentioned above. For example, Bakre and Jangid (2007) presented the optimal values when the mass ratio is up to 0.1. For ease of use in practical applications, in the present study, the optimal parameters for the high mass ratio up to 0.9 are underlined and tabulated in Table 3.

3.3. Sensitivity analyses

The optimal values estimated in Table 3 are based on a given mass ratio (μ) and the damping ratio (ζ_o) of the main structure. In real engineering practices, some uncertainties inevitably exist. For example, marine growth surrounding the outer pipe can change the mass ratio of the system and can also influence the damping ratio of the main structure. The robustness of the system is therefore important. To demonstrate the robustness of the system, four different mass ratios (μ = 0.05, 0.1, 0.4, 0.9) are considered. In each case, the damping ratio (ζ_o) of the main oscillator is kept the same; specifically ζ_o = 0.031, the same value as in Exp. 1 in Table 1. Fig. 6 and Fig. 7 show the variation and contour of the response optimization index (N) against different TMD parameters. The results demonstrate that mass ratio significantly influences the robustness of the system. When the mass ratio is small (e.g. in Fig. 6(a) and (b)), the smallest optimization index can be obtained only within a very narrow range. This is why it is generally reported that the control effectiveness of the conventional-TMD system is sensitive to the mass ratio (e.g. Hoang et al. (2008) and Reggio and Angelis (2015)). When the mass ratio becomes larger (e.g. in Fig. 6(c) and (d)), the results become rather flat around the minimum value N^{opt}, which means the system will be effective even if the parameters shift away from the optimal values. For the PIP system, the mass ratio can reach more than 80% (e.g. Bi and Hao (2016)), this property will significantly facilitate the design of the connecting device (which is represented by a spring and dashpot in the analytical model) within the annulus of the PIP system.

In Fig. 6 and Fig. 7, a damping ratio of ζ_o = 0.031 is assumed. The optimum index (N^{opt}) with different damping ratio is shown in Fig. 8. As shown, increasing the damping of the main oscillator leads to better performance of the structure-TMD system (lower values of N^{opt}) and when the mass ratio is large, the influence of damping ratio becomes less evident. These results again demonstrate the robustness of the non-conventional TMD system to suppress undesired vibrations.

3.4. Explicit formulae for optimum TMD parameters

In this section, for easy use in engineering applications, explicit mathematical expressions for optimal tunning parameters for a non-conventional structure-TMD system under an external force are estimated by a curve fitting scheme. The tuning results obtained from the numerical searching technique are shown in Fig. 9 and Fig. 10. It can be seen that ζ_o slightly influence f^{opt} while it almost has no effect on ζ_i^{opt}. Eqs. (17) and (18) are obtained by using the surface curve fitting in MATLAB.

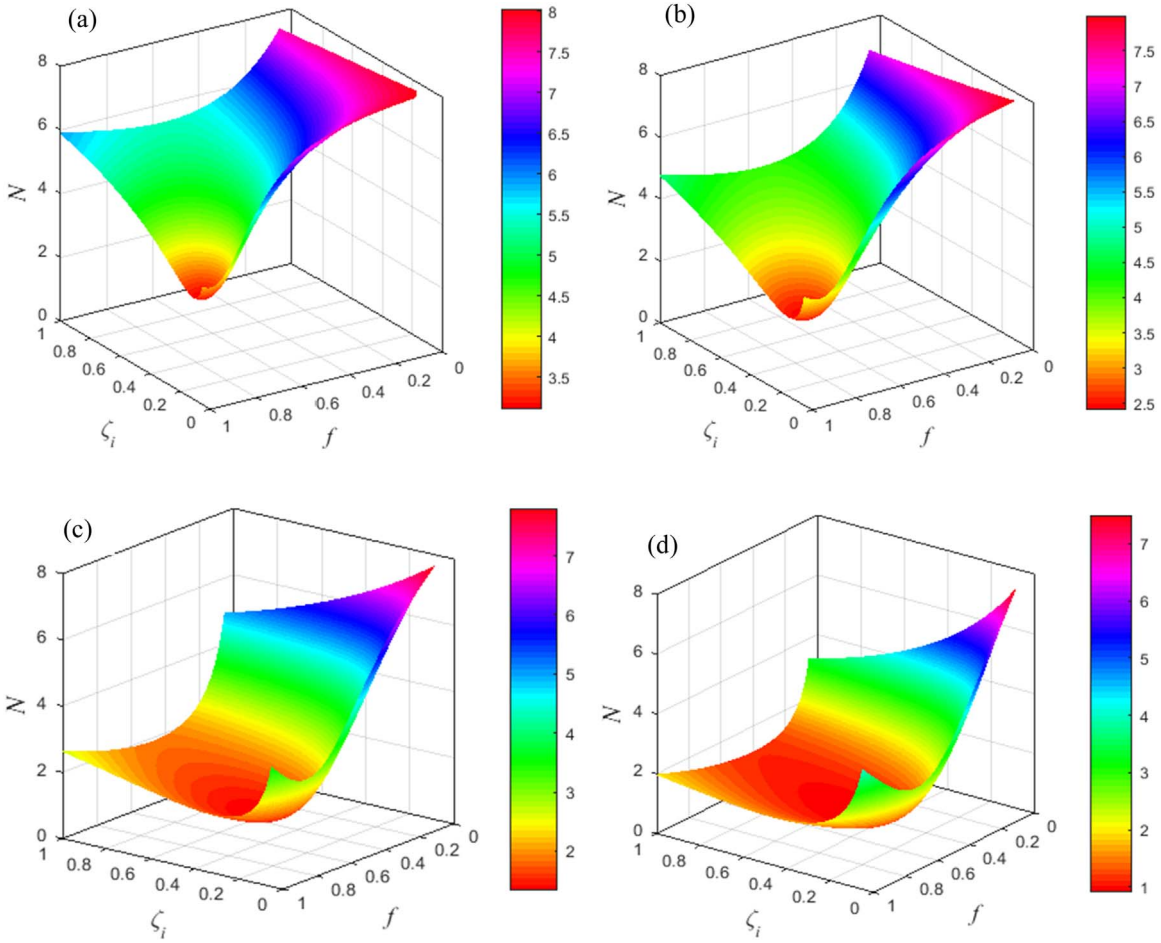

Fig. 6. Mean square displacement response index (N) of a main system with different TMD masses. (a) μ = 0.05; (b) μ = 0.1; (c) μ = 0.4; (d) μ = 0.9. (ζ_o = 0.031).

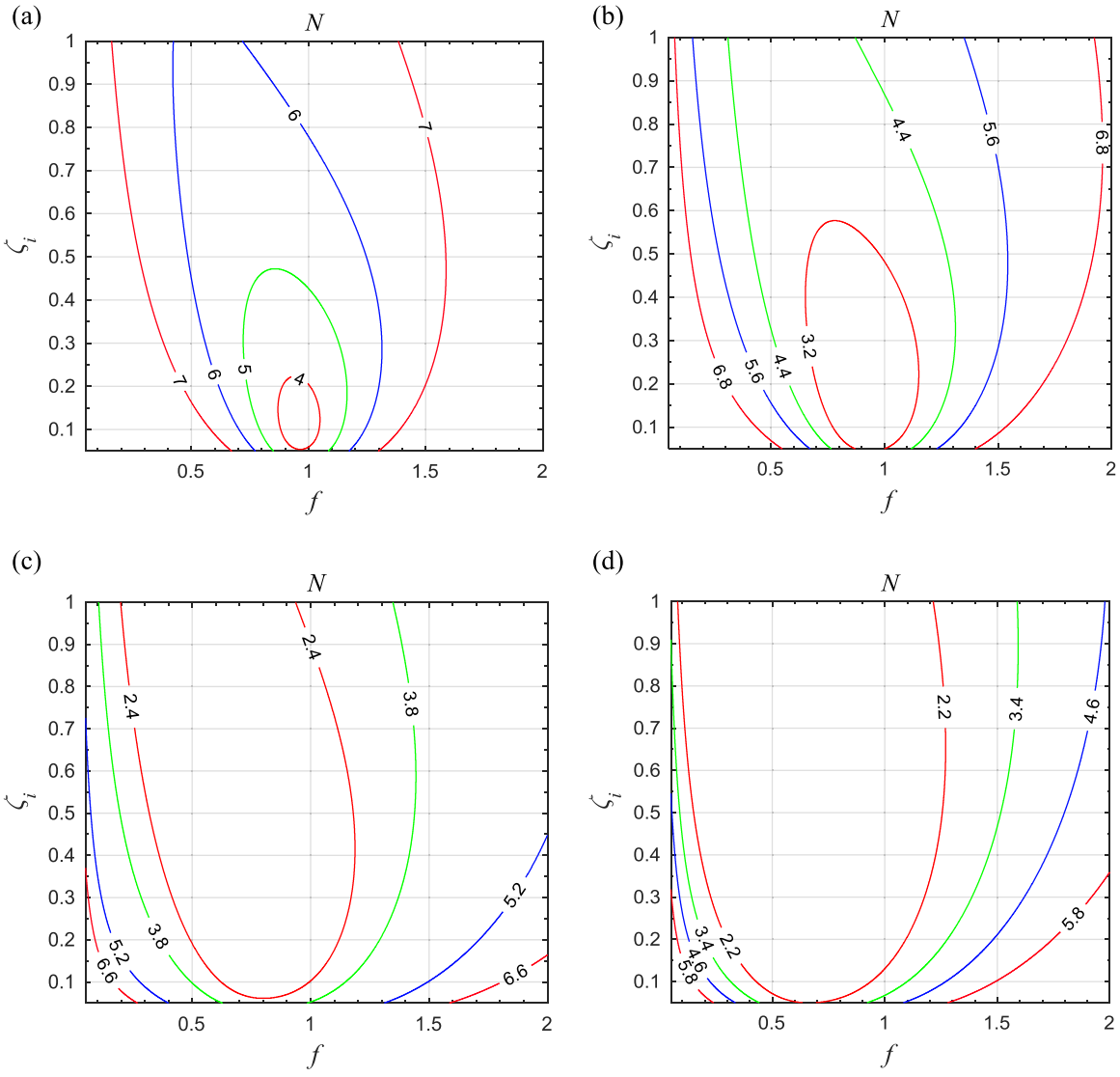

Fig. 7. Intensity contour of N of a main system with different TMD masses. (a) $\mu = 0.05$; (b) $\mu = 0.1$; (c) $\mu = 0.4$; (d) $\mu = 0.9$. ($\zeta_o = 0.031$).

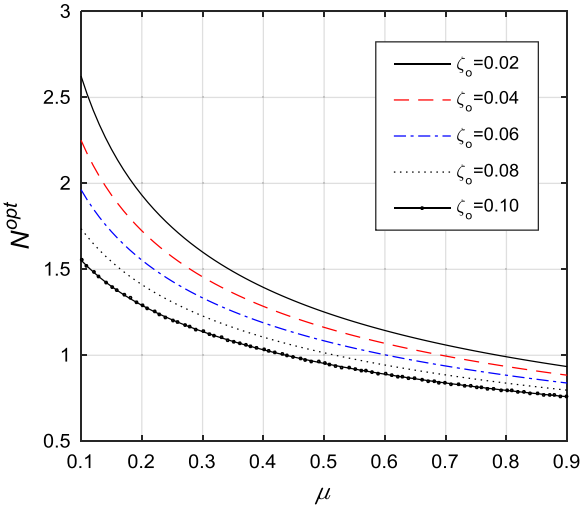

Fig. 8. Influence of damping ratio on the optimum index.

$$f^{opt} = 1.093 - 0.4814\sqrt{\mu} - 0.06\sqrt{\zeta_o} \quad (17)$$

$$\zeta_i^{opt} = 0.1\ln(\mu) + 0.375 \quad (18)$$

R-square, which reflects the reliability of the curve fitting (R=1 means accurate estimation of the values), reach 0.999 and 0.995, respectively in the present study.

4. Effectiveness of optimized PIP system to mitigate VIV of cylindrical structures

This section investigates the effectiveness of using modified PIP system to mitigate VIV. The cylindrical structure tested in (Rahman, 2015; Rahman and Thiagarajan, 2013) is adopted again. However, the single pipe in the test is divided into two pipes in order to form a PIP system. For these two systems, the total mass of the pipe(s) is kept the same. For example, if the mass of the single pipe is m, the masses of the outer and inner pipes can be determined by the mass ratio as $m_o = m/(1+\mu)$ and $m_i = m - m_o$. As discussed before, the mass ratio of a PIP system can be quite large and without losing generality, a mass ratio of $\mu = 0.8$ and $\zeta_o = 0.031$ are assumed in the present study to demonstrate the

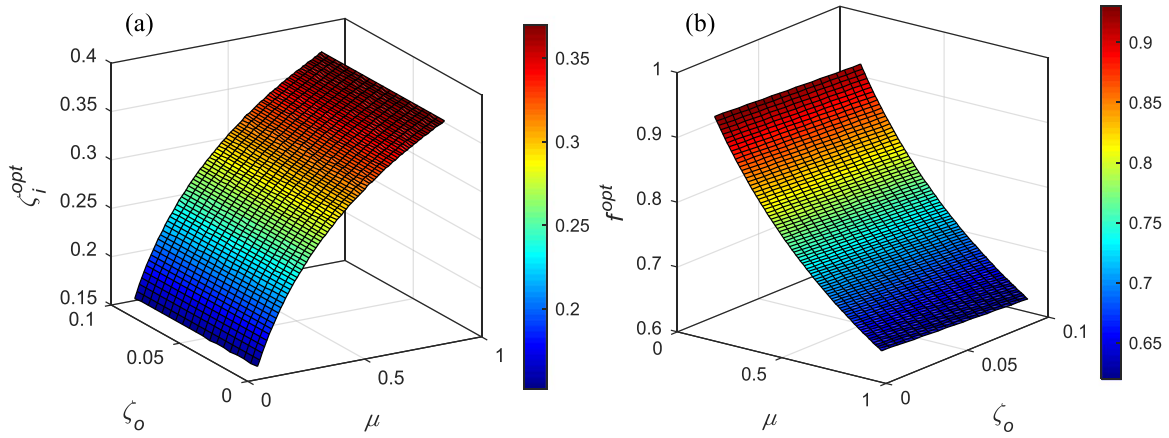

Fig. 9. Optimum tuning parameters obtained from numerical searching scheme: (a) optimum TMD damping ratio (ζ_i^{opt}) and (b) optimum tuning frequency ratio (f^{opt}).

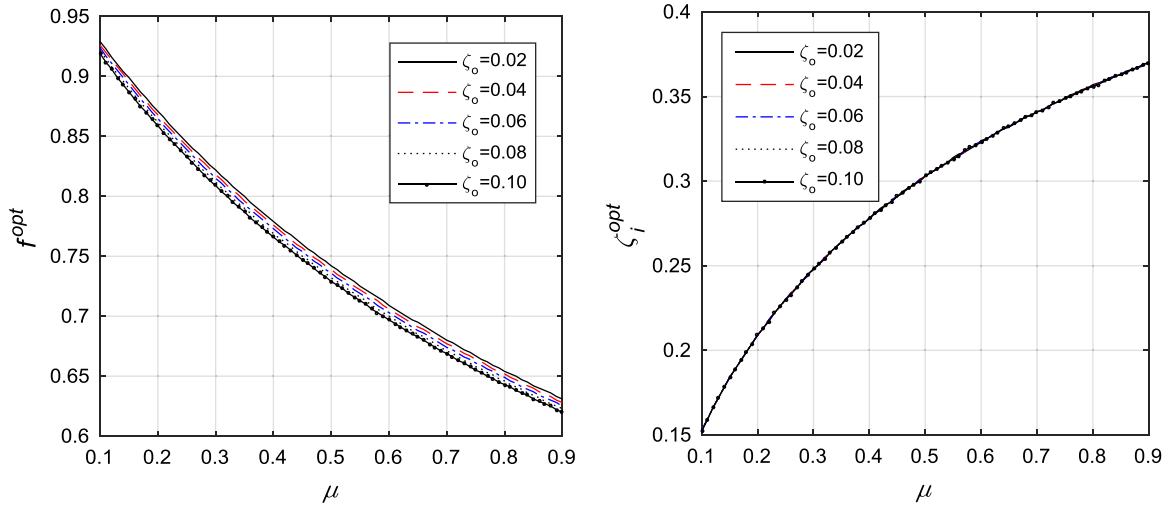

Fig. 10. Variation of optimum tuning parameters as a function of mass ratio (μ) for various damping ratios of main system (ζ_o).

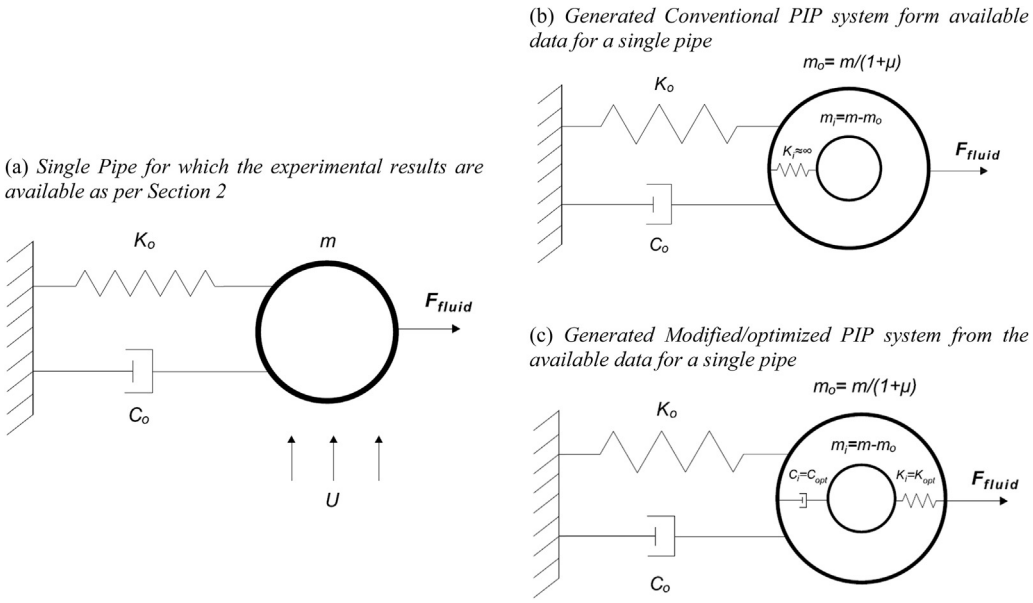

Fig. 11. Different pipe models under VIV: (a) A single pipe as presented in Section 2, (b) a PIP system connected by a very rigid spring and (c) a modified PIP system with the optimized parameters.

effectiveness of the proposed design. It should be noted that by dividing a single pipe into two, the thicknesses of each pipe becomes smaller, which may cause certain problems in real applications. For example, the thinner external pipe may not be enough to withstand the external hydrostatic pressure when it is submerged. However, the purpose of this paper is to investigate the

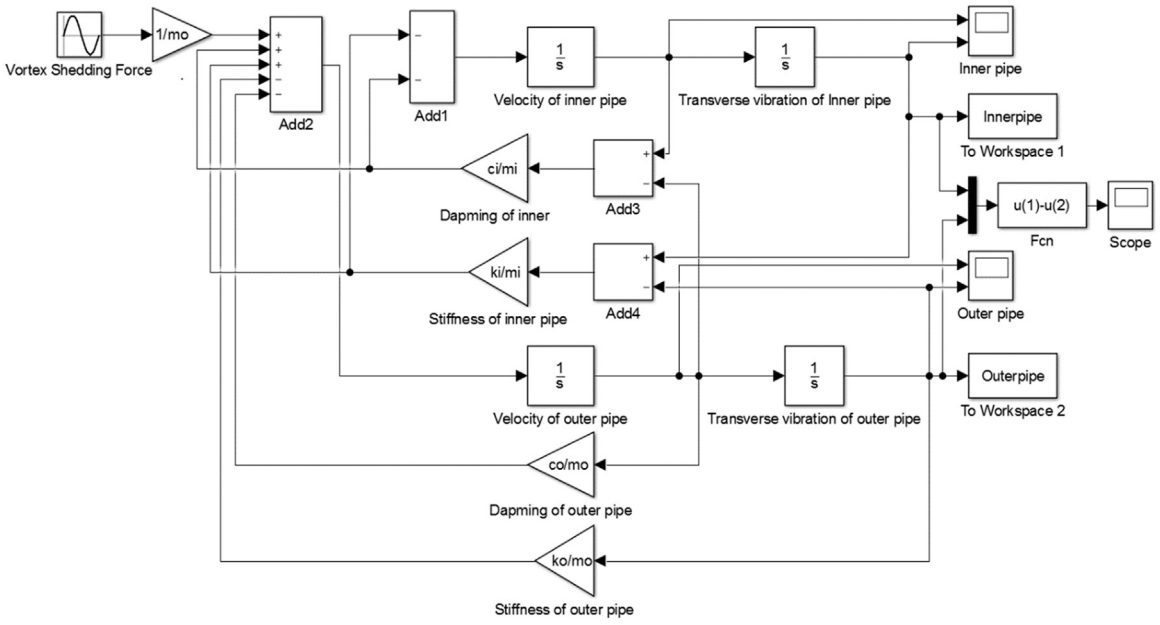

Fig. 12. The dynamic Simulink model for a modified PIP system under VIV.

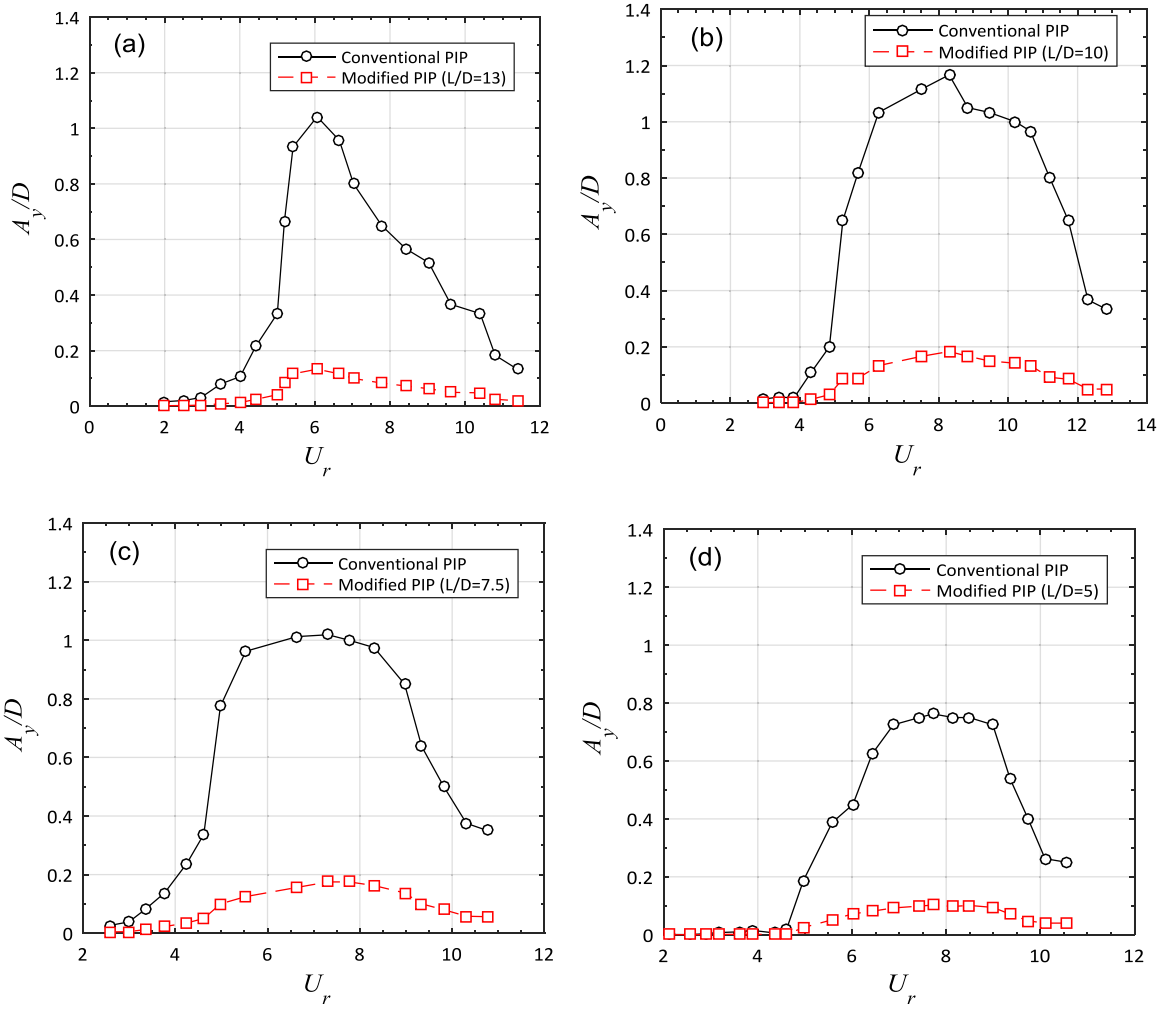

Fig. 13. Comparisons of normalized transverse vibration amplitudes of a single pipe system with the optimized PIP system. (a) $L/D = 13$; (b) $L/D = 10$; (c) $L/D = 7.5$; (d) $L/D = 5$. (For interpretation of the references to color in this figure, the reader is referred to the web version of this article)

Table 4
Peak normalized amplitudes of the single pipe model and the optimized PIP system under VIV and the corresponding suppression ratio.

Aspect ratio (L/D)	Single pipe	Optimized PIP	Suppression ratio
13	1.04	0.13	87%
10	1.17	0.18	84%
7.5	1.02	0.17	82%
5	0.76	0.10	86%

effectiveness of the proposed concept, therefore, such problems are not considered in the present study.

Fig. 11(a) shows the single pipe tested in Rahman (2015) and Rahman and Thiagarajan (2013). Fig. 11(b) and (c) show the modified PIP systems. A very stiff spring ($k_i \simeq \infty$) is used to connect the inner and outer pipes in Fig. 11(b). These two pipes will therefore vibrate together when they are subjected to VIV and this system actually becomes the same as that of Fig. 11(a). In Fig. 11(c), the optimal spring and dashpot are used to connect the inner and outer pipes. Relative displacement is allowed between the inner and outer pipes and this system can be simplified as a structure-TMD system as mentioned above. In the present study, the optimal tuning frequency and damping ratio can be estimated as $f^{opt} = 0.65$ and $\zeta_i^{opt} = 0.35$ according to Eqs. (17) and (18).

The equation of motion of the proposed PIP system (a two-DoF system) has been derived in Section 3 and can be represented by Eq. (7). To solve this equation, a time-domain Simulink model is developed in MATLAB again and shown in Fig. 12. To validate this model, the vibration of the system shown in Fig. 11(b) is calculated and compared with those obtained in Fig. 4 (the red curves). Exactly same results are obtained. The accuracy of this Simulink model is therefore validated and it is applied to calculate the PIP response shown in Fig. 11(c). It should be noted that the same C_F values as shown in Fig. 2 are used for different pipe systems.

Fig. 13 compares the normalized cross-flow fluctuations of the single pipe and the optimized PIP systems. The dark curves are the results obtained from the single pipe model and the red curves are from the optimized PIP system. Fig. 13 clearly shows that with the optimized PIP system, the vibration induced by vortex shedding can be significantly suppressed within all the considered reduced velocities. In other words, this system is not sensitive to the frequency of excitation ($f_{vortex} = S_t U/D$). This is because the mass ratio of this PIP system is quite large, and it is not sensitive to the external vibration sources as discussed in Section0 3.3. It should be mentioned that for PIP system, similar to single pipe (Section 2.2), reduced velocity is defined as $U_r = U/f_n D$.

Table 4 tabulates the maximum amplitudes for different systems and the corresponding reduction ratios. It can be seen that the maximum reduction ratio can reach 87% when the aspect ratio is 13. Aspect ratio seems only slightly influence the control efficiency. For the investigated cases the reduction ratios are more or less the same with an average value about 84%.

5. Possible practical design options

In this paper, analytical studies are carried out to examine the effectiveness of using PIP system to mitigate VIV. The connecting device is crucial for the design and it is simplified as a spring and dashpot in the present study. In engineering practical, polyurethane foam (PUF) or rotational friction hinge device with spring (RFHDS) as suggested in Bi and Hao (2016) might be the options to provide the required stiffness and damping of the connecting device. Further experimental studies will be carried out in the next step to find the most appropriate option.

6. Conclusion

This paper proposes using modified PIP system to mitigate vortex induced vibrations of cylindrical offshore components such as risers and deep sea pipelines. The effectiveness of the proposed method is investigated through analytical solutions by simplifying the system as a structure-TMD system. The equation of motion of the PIP system is derived and implemented into the MATLAB/Simulink code and validated by the experimental data. The optimal parameters for the connecting spring and dashpot are calculated and explicit formulae for these parameters are derived. Analytical results show that VIV can be significantly suppressed by the proposed PIP system and this system is not sensitive to the external excitation frequency contents and variations of the mass ratio. This system is believed having great application potentials to control VIV of offshore cylindrical components.

Acknowledgement

The authors would like to acknowledge the support from Australian Research Council Discovery Early Career Researcher Award (DECRA) DE150100195 for carrying out this research.

References

Allen, D., 2003. Performance characteristics of short fairings. In: Proceedings of the Offshore Technology Conference, Houston, Texas, USA, pp. 1–9.
Alrsai, M., Karampour, H., 2016. Propagation buckling of pipe-in-pipe systems, an experimental study. In: Proceedings of the 20th ISOPE Pacific/Asia Offshore Mechanics Symposium. International Society of Offshore and Polar Engineers, Gold Coast, Australia, pp. 408–413.
Anh, N.D., Nguyen, N.X., 2013. Design of TMD for damped linear structures using the dual criterion of equivalent linearization method. Int. J. Mech. Sci. 77, 164–170.
Assi, G.R.S., Bearman, P.W., Kitney, N., 2009. Low drag solutions for suppressing vortex-induced vibration of circular cylinders. J. Fluids Struct. 25 (4), 666–675.
Azmi, A.M., Zhou, T., Cheng, L., Wang, H., Chua, L.P., 2012. On the effectiveness and mechanism of vortex-induced vibration suppression using a screen cylinder. In: Proceedings of the 22nd International Offshore and Polar Engineering Conference. International Society of Offshore and Polar Engineers, Rhodes, Greece, pp. 586–594.
Bai, Y., Bai, Q., 2005. Subsea Pipelines and Risers. Elsevier.
Bai, Y., Bai, Q., 2012. Subsea Engineering Handbook. Gulf Professional Publishing.
Bakre, S., Jangid, R., 2007. Optimum parameters of tuned mass damper for damped main system. Struct. Control Health Monit. 14 (3), 448–470.
Bekdaş, G., Nigdeli, S.M., 2011. Estimating optimum parameters of tuned mass dampers using harmony search. Eng. Struct. 33 (9), 2716–2723.
Bernitsas, M.M., Raghavan, K., 2014. Reduction of Vortex Induced Forces and Motion through Surface Roughness Control. Google Patents.
Bi, K., Hao, H., 2016. Using pipe-in-pipe systems for subsea pipeline vibration control. Eng. Struct. 109, 75–84.
Choi, H., Jeon, W.P., Kim, J., 2008. Control of Flow over a Bluff Body, Annual Review of Fluid Mechanics. Annual Reviews, Palo Alto, pp. 113–139.
Dinh, V.N., Basu, B., 2015. Passive control of floating offshore wind turbine nacelle and spar vibrations by multiple tuned mass dampers. Struct. Control Health Monit. 22 (1), 152–176.
Facchinetti, M.L., De Langre, E., Biolley, F., 2004. Coupling of structure and wake oscillators in vortex-induced vibrations. J. Fluids Struct. 19 (2), 123–140.
Farshidianfar, A., Zanganeh, H., 2010. A modified wake oscillator model for vortex-induced vibration of circular cylinders for a wide range of mass-damping ratio. J. Fluids Struct. 26 (3), 430–441.
Gabbai, R., Benaroya, H., 2005. An overview of modeling and experiments of vortex-induced vibration of circular cylinders. J. Sound Vib. 282 (3), 575–616.
Gad-el-Hak, M., 2000. Flow Control: Passive, Active and Reactive Flow Management. Cambridge Univ. Press, UK.
Gao, Y., Fu, S., Wang, J., Song, L., Chen, Y., 2015. Experimental study of the effects of surface roughness on the vortex-induced vibration response of a flexible cylinder. Ocean Eng. 103, 40–54.
Gao, Y., Yang, J., Xiong, Y., Wang, M., Peng, G., 2016. Experimental investigation of the effects of the coverage of helical strakes on the vortex-induced vibration response of a flexible riser. Appl. Ocean Res. 59, 53–64.
Goswami, I., Scanlan, R.H., Jones, N.P., 1993. Vortex-induced vibration of circular cylinders. II: new model. J. Eng. Mech. 119 (11), 2288–2302.
Gouda, B., 1975. Some Measurements of the Phenomena of Vortex Shedding and Induced Vibrations of Circular Cylinder. Technische Universitat Berlin Report DLR-FB, 75-01.
Gutierrez Soto, M., Adeli, H., 2013. Tuned mass dampers. Arch. Comput. Methods Eng. 20 (4), 419–431.
Hoang, N., Fujino, Y., Warnitchai, P., 2008. Optimal tuned mass damper for seismic applications and practical design formulas. Eng. Struct. 30 (3), 707–715.
ISO, 2015. 19901-1: 2015, Petroleum and Natural Gas Industries-specific Requirements

for Offshore Structures-Part 1: Metocean Design and Operating Conditions. British Standards Institute.
Khorasanchi, M., Huang, S., 2014. Instability analysis of deepwater riser with fairings. Ocean Eng. 79, 26–34.
Kiu, K.Y., Stappenbelt, B., Thiagarajan, K.P., 2011. Effects of uniform surface roughness on vortex-induced vibration of towed vertical cylinders. J. Sound Vib. 330 (20), 4753–4763.
Kumar, R.A., Sohn, C.-H., Gowda, B.H., 2008. Passive control of vortex-induced vibrations: an overview. Recent Pat. Mech. Eng. 1 (1), 1–11.
Kyriakides, S., 2002. Buckle propagation in pipe-in-pipe systems.: Part I. experiments. Int. J. Solids Struct. 39 (2), 351–366.
Nakamura, T., Kaneko, S., Inada, F., Kato, M., Ishihara, K., Nishihara, T., Mureithi, N.W., Langthjem, M.A., 2013. Flow-induced Vibrations: Classifications and Lessons from Practical Experiences. Butterworth-Heinemann.
Norberg, C., 1994. An experimental investigation of the flow around a circular cylinder: influence of aspect ratio. J. Fluid Mech. 258, 287–316.
Owen, J.C., Bearman, P.W., Szewczyk, A.A., 2001. Passive control of VIV with drag reduction. J. Fluids Struct. 15 (3), 597–605.
Park, H., Bernitsas, M.M., Ajith Kumar, R., 2012. Selective roughness in the boundary layer to suppress flow-induced motions of circular cylinder at 30,000 < Re < 120,000. J. Offshore Mech. Arct. Eng. 134 (4), (041801-041801).
Raghavan, A.K., Chan-Hyun, S., Bangalore, H.L.G., 2008. Passive control of vortex-induced vibrations: an overview. Recent Pat. Mech. Eng. 1 (1), 1–11.
Rahman, M.A., 2015. Vortex-induced Vibration of Circular Cylindrical Structure with Different Aspect Ratios, Mechanical Engineering. University of Western Australia.
Rahman, M.A., Thiagarajan, K., 2013. Vortex-induced vibration of cylindrical structure with different aspect ratio. In: The 23th International Offshore and Polar Engineering Conference. International Society of Offshore and Polar Engineers, Anchorage, Alaska, USA, pp. 395–401.
Rahman, M.A.A., Leggoe, J., Thiagarajan, K., Mohd, M.H., Paik, J.K., 2016. Numerical simulations of vortex-induced vibrations on vertical cylindrical structure with different aspect ratios. Ships Offshore Struct. 11 (4), 405–423.
Rashidi, S., Hayatdavoodi, M., Esfahani, J.A., 2016. Vortex shedding suppression and wake control: a review. Ocean Eng. 126, 57–80.
Reggio, A., Angelis, M.D., 2015. Optimal energy-based seismic design of non-conventional Tuned Mass Damper (TMD) implemented via inter-story isolation. Earthq. Eng. Struct. Dyn. 44 (10), 1623–1642.
Saint-Marcoux, J.-F., 2014. Recent trends and future of ultra deepwater oil fields. In: Proceedings of the 24th International Ocean and Polar Engineering Conference. International Society of Offshore and Polar Engineers, Busan, Korea, pp. 1–8.
Salvi, J., Rizzi, E., 2015. Optimum tuning of tuned mass dampers for frame structures under earthquake excitation. Struct. Control Health Monit. 22 (4), 707–725.
Sarpkaya, T., 2004. A critical review of the intrinsic nature of vortex-induced vibrations. J. Fluids Struct. 19 (4), 389–447.
Song, L., Fu, S., Cao, J., Ma, L., Wu, J., 2016. An investigation into the hydrodynamics of a flexible riser undergoing vortex-induced vibration. J. Fluids Struct. 63, 325–350.
Szepessy, S., Bearman, P., 1992. Aspect ratio and end plate effects on vortex shedding from a circular cylinder. J. Fluid Mech. 234, 191–217.
Veritas, N., 2000. Environmental Conditions and Environmental Loads. Det Norske Veritas.
Wang, Z., Chen, Z., Liu, H., 2015. Numerical study on upheaval buckling of pipe-in-pipe systems with full contact imperfections. Eng. Struct. 99, 264–271.
Williamson, C., Govardhan, R., 2004. Vortex-induced vibrations. Annu. Rev. Fluid Mech. 36, 413–455.
Williamson, C.H.K., Govardhan, R., 2008. A brief review of recent results in vortex-induced vibrations. J. Wind Eng. Ind. Aerodyn. 96 (6–7), 713–735.
Zeinoddini, M., Farhangmehr, A., Seif, M.S., Zandi, A.P., 2015. Cross-flow vortex induced vibrations of inclined helically straked circular cylinders: an experimental study. J. Fluids Struct. 59, 178–201.
Zhao, M., Cheng, L., 2010. Finite element analysis of flow control using porous media. Ocean Eng. 37 (14–15), 1357–1366.
Zheng, J., Palmer, A., Brunning, P., Gan, C.T., 2014. Indentation and external pressure on subsea single wall pipe and pipe-in-pipe. Ocean Eng. 83, 125–132.
Zhou, T., Razali, S.F.M., Hao, Z., Cheng, L., 2011. On the study of vortex-induced vibration of a cylinder with helical strakes. J. Fluids Struct. 27 (7), 903–917.
Zhu, H., Yao, J., 2015. Numerical evaluation of passive control of VIV by small control rods. Appl. Ocean Res. 51, 93–116.